Tetrahedron 73 (2017) 4610–4615

Contents lists available at ScienceDirect

Tetrahedron

journal homepage: www.elsevier.com/locate/tet

Novel hole transport materials based on triarylamine/naphtho[2,1-*b*] benzofunan for efficient green electroluminescent device

Panpan Wu [a], Guojian Tian [a], Mingming Hu [a], Hong Lian [b], Qingchen Dong [b, **], Wenting Liang [c, ***], Jinhai Huang [a, d, *], Jianhua Su [a]

[a] Key Laboratory for Advanced Materials and Institute of Fine Chemicals, East China University of Science & Technology, Shanghai, 200237, PR China
[b] Ministry of Education Key Laboratory of Interface Science and Engineering in Advanced Materials, Research Center of Advanced Materials Science and Technology, Taiyuan University of Technology, Taiyuan, 030024, PR China
[c] Institute of Environmental Science, Shanxi University, Taiyuan, 030006, PR China
[d] Shanghai Taoe Chemical Technology Co., Ltd, Shanghai, PR China

ARTICLE INFO

Article history:
Received 18 April 2017
Received in revised form
7 June 2017
Accepted 16 June 2017
Available online 17 June 2017

Keywords:
naphtho[2,1-*b*]benzofunan
Hole transport
Stable
Efficient

ABSTRACT

Two hole transport materials, N-([1,1'-biphenyl]-4-yl)-9,9-dimethyl-N-(4-(naphtho[2,1-*b*]benzofuran-6-yl)phenyl)-9H-fluoren-2-amine (DFA) and N-(9,9-dimethyl-9H-fluoren-2-yl)-9,9-dimethyl-7-(naphtho[2,1-*b*]benzofuran-6-yl)-N-phenyl-9H-fluoren-2-amine (TFA) were designed, synthesized and fully characterized. The photophysical and thermal properties of these two compounds were investigated by UV–vis absorption spectra, photoluminescence spectra, thermogravimetric analysis (TGA) and differential scanning calorimetry analysis (DSC), which indicated that DFA and TFA would be efficient hole transport materials due to their proper HOMO energy levels and excellent thermal stability. Then, green OLEDs with DFA and TFA as hole transport layer, respectively, were fabricated, NPB-based OLEDs was also prepared for comparison. It turned out that DFA- and TFA-based devices exhibited higher efficiencies than that of NPB-based device, and TFA-based device showed the best performances with current efficiency, power efficiency and external quantum efficiency of 41.68 cd/A, 32.04 lm/W and 12.04%, respectively.

1. Introduction

Organic light- emitting diodes(OLEDs) have caused extensive and strong attention since the first efficient OLED presented by the research group of Tang,[1] which is mainly attributed to their properties of small volume, fast response, high luminous efficiency and large view angle, etc.[2–5] The initial OLED was called single-layer device due to the simple constitution of anode, emitting layer and cathode. With the rapid development of scientific research, the construction of OLED has been improved. To date, organic light-emitting devices are generally fabricated of anode, hole transport layer(HTL), emitting layer, electron transport layer(ETL) and cathode. The improved OLEDs can achieve higher carrier injection efficiencies than single-layer device.[6,7] Novel OLEDs have become vital segment of flat panel displays and lighting equipment.[8–12] In the past decades, great development has been achieved in OLED materials and devices, however there are some crucial problems to be solved.[13–16]

Hole transport materials are one of the key factor for high efficient organic light-emitting diodes, which play the roles of hole transporter and electron blocker between hole injection layer and emitting layer. The proper highest occupied molecular orbital(HOMO) energy level, good thermal stability and excellent film-forming property are necessary for a satisfied hole transport material.[17–21] Triarylamine type compounds are ideal hole transport materials for OLEDs, which possess high thermal stability, appropriate HOMO energy level and good solubility.[22–25] N,N'-bis-(3-methylphenyl)-N,N'-bis-phenyl-benzidine(TPD) and N,N'-di(naphthalen-1-yl)-N,N'-diphenyl-[1,1'-biphenyl]-4,4'-diamine (NPB) are among the most familiar hole transport materials due to their excellent hole-transport property, although their poor thermal stability is an obvious defect of them.[26–28] For this reason, new

* Corresponding author. Key Laboratory for Advanced Materials and Institute of Fine Chemicals, East China University of Science & Technology, Shanghai, 200237, PR China.
** Corresponding author.
*** Corresponding author.
E-mail addresses: dongqingchen@tyt.edu.cn (Q. Dong), liangwt@sxu.edu.cn (W. Liang), dele12@163.com (J. Huang).

http://dx.doi.org/10.1016/j.tet.2017.06.031
0040-4020/

hole transport materials need to be explored.

In this work, two triarylamine-based hole transport materials, N-([1,1'-biphenyl]-4-yl)-9,9-dimethyl-N-(4-(naphtho[2,1-b] benzofuran-6-yl)phenyl)-9H-fluoren-2-amine(DFA) and N-(9,9 dimethyl-9H-fluoren-2-yl)-9,9-dimethyl-7-(naphtho[2,1-b] benzofuran-6-yl)-N-phenyl-9H-fluoren-2-amine(TFA) were designed and synthesized. According to literature,[29] benzofuran moiety is an ideal electron acceptor with excellent stability, while dibenzo[*b*,*d*]furan moiety can decrease the oxidation potential and increase the number of delocalized electrons, thus enhancing the HOMO energy level and facilitating the transport of hole excitons. Thus, we guessed that the addition of benzene ring on dibenzofuran moiety can increase the molecular weight, which can improve the thermal stabilities and amorphous state of compounds, thereby realizing excellent device performance of the corresponding OLEDs. Based on the above considerations, the naphtho[2,1-*b*]benzofuran was introduced to the structure of these three compounds, which can boost the molecular planarity and thermal stability. To verify the hole transport capacity of these two triarylamine compounds, OLED devices using DFA and TFA as hole transport materials were fabricated, and evaluated by comparing with NPB based device in the same structure.

2. Result and discussion

2.1. Synthesis and characterization

The synthetic routes of the intermediates and target compounds were shown in Scheme 1. Firstly, the naphtho[2,1-*b*]benzofuran was treated with n-BuLi at −78 °C, followed by reaction with boric acid triisopropyl ester to give rise to the compound **3**. The intermediates **1** and **2** were synthesized by Buchwald–Hartwig and Ullmann reaction according to procedure as reported in literature. The target products were prepared by Suzuki coupling reaction, then purified by flash column chromatography and recrystallization method with yields of 68% and 92.53%, respectively. The molecule structures of these compounds were characterized by ^{1}H NMR, ^{13}C NMR, and high-resolution mass spectrometry(HRMS).

2.2. Photophysical properties

The absorption and emission spectra of DFA and TFA were measured in tetrahydrofuran solution. As shown in Fig. 1 and Table 1, the stronger UV–Vis absorption peaks of DFA and TFA are similarly located at around 278 nm, which is attributed to the π-π*

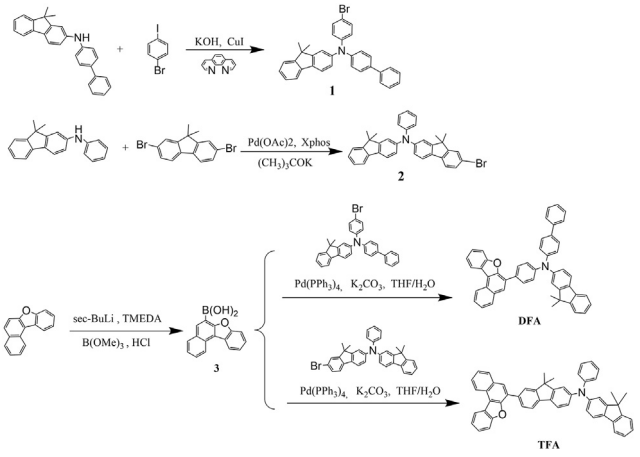

Scheme 1. Synthetic routes of the compounds.

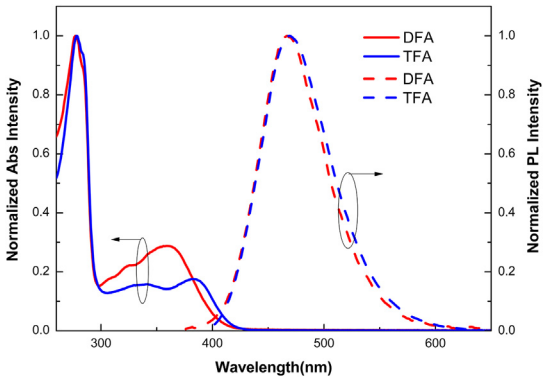

Fig. 1. Normalized UV–vis absorption and fluorescence emission spectra of the compounds in tetrahydrofuran solution at room temperature.

transitions of the conjugated aromatic segments, the weaker absorption peaks for DFA and TFA are respectively located at around 359 nm and 382 nm, which should be derived from the n-π* transitions for the extended conjugation of triarylamine and naphtho[2,1-*b*]benzofuran. The optical energy bandgaps (E_g) of these two compounds are calculated to be 3.05 eV and 3.01 eV, respectively, through calculation from the onset of the absorption spectra. The maximum PL emission peak was located at 467 nm and 469 nm for DFA and TFA, respectively. The mild red-shifted photoluminescence spectrum of TFA compared to that of DFA could be ascribed to the larger conjugation of TFA.

2.3. Thermal properties

The thermal properties of DFA and TFA were investigated by thermogravimetric analysis (TGA) and differential scanning calorimetry analysis (DSC) under nitrogen atmosphere with a heating rate of 10 °C/min. As shown in Fig. 2a, the decomposition temperatures (T_d), which correspond to 5% weight loss, were measured to be 426 and 408 °C for DFA and TFA, respectively. Meanwhile, their corresponding glass transition temperatures (T_g) can be found from DSC curves (Fig. 2b), which were determined to be 122 and 129 °C for DFA and TFA, respectively. In addition, the whole DSC analysis of DFA and TFA are showed in Fig. S1 and Fig. S2, respectively, the first heating eliminated thermal history of these two materials, and the second heating revealed the original property of these two materials. Powder XRD did not reveal any sharp reflections (Fig. S3 and Fig. S4). Hence, XRD and the excellent thermal behaviors indicate that these two materials are amorphous and thermally stable. The decomposition (T_d) and glass transition (T_g) temperatures are summarized in Table 1.

2.4. Electrochemical properties

The electrochemical behaviors of these two compounds were investigated by cyclic voltammograms (CV) using a standard three-electrode electrochemical cell in an electrolyte solution (0.1M TBAPF6/DCM), with ferrocene as external reference. The CV curves of DFA and TFA were shown in Fig. 3, from which the highest occupied molecular orbital (HOMO) energy level of DFA and TFA were calculated to be −5.22eV and −5.19eV, respectively. The lowest unoccupied molecular orbital (LUMO) were then determined to be −2.17eV and −2.18eV, respectively, through the equation of $E_{LUMO} = E_{HOMO} + E_g$. The high HOMO energy levels imply that these two compounds would be ideal hole transport materials.

Table 1
The physical properties of **DFA** and **TFA**.

Compounds	λ_{abs}(nm)[a]	λ_{em}(nm)[a]	E_g(eV)[b]	HOMO(eV)[c]	LUMO(eV)[d]	T_g(°C)[e]	T_d(°C)[f]
DFA	359	467	3.05	−5.22	−2.17	122	426
TFA	382	469	3.01	−5.19	−2.18	129	408

[a] Measured in tetrahydrofuran at a concentration of 1.0×10^{-5}.
[b] Estimated from onset of the absorption spectra ($E_g = 1241/\lambda_{onset}$).
[c] The HOMO energy level was measured from cyclic voltammetry ($E_{HOMO} = -4.4 - E_{ox}$).
[d] The LUMO energy level was measured by the equation: $E_{LUMO} = E_{HOMO} + E_g$.
[e] Measured by DSC curves.
[f] Measured by TGA curves.

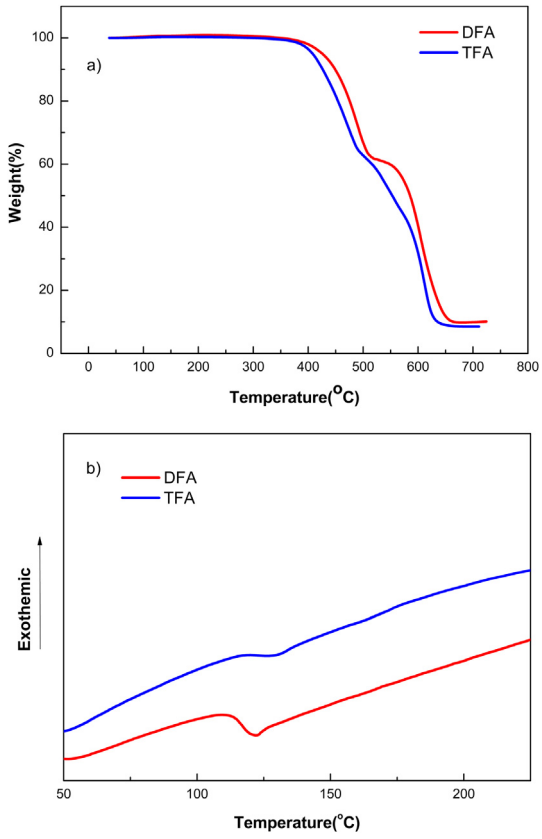

Fig. 2. a). The thermogravimetric analysis (TGA) curves, the decomposition temperatures (T_d) corresponding to 5% weight loss; b) Differential scanning calorimetry (DSC) curves of DFA and TFA.

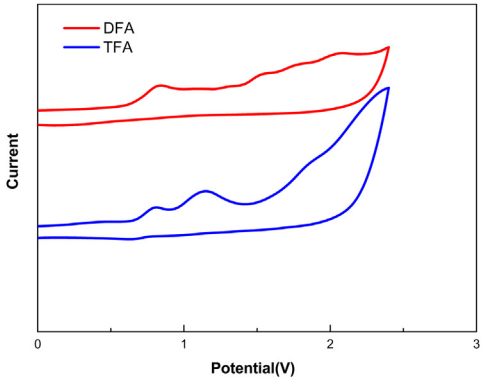

Fig. 3. Cyclic voltammograms of the three compounds in dichloromethane.

2.5. EL performance

To investigate the hole-transporting properties of these two triarylamine-based materials, OLEDs with the device structure of [ITO/MoO_3 (3 nm)/HTM (40 nm)/TCTA (10 nm)/CBP:Ir(ppy)$_3$ (20 nm, 8 wt%)/TPBi (35 nm)/LiF (1 nm)/Al (200 nm)] were fabricated using DFA or TFA as the hole-transport layer, ITO and LiF/Al were employed as the anode and composite cathode, respectively. MoO_3, TCTA and TPBi acted as hole injection layer(HIL), electron block layer(EBL) and electron transport layer(ETL), respectively. CBP was played as host, and Ir(ppy)$_3$ was used as the emitting material. For comparison, the control device with configuration of [ITO/MoO_3 (3 nm)/NPB (40 nm)/TCTA (10 nm)/CBP:Ir(ppy)$_3$ (20 nm, 8 wt %)/TPBi (35 nm)/LiF (1 nm)/Al (200 nm)] was also prepared. The energy level diagram of these materials in as-prepared devices are shown in Fig. 4.

The current density-voltage-luminance (I-V-L) characteristics of these devices with various hole transport materials are shown in Fig. 5, and related data are summarized in Table 2. It can be seen that, the turn-on voltages of these devices were small, which were determined to be 2.9–3.6 V, meanwhile, the current density and luminance of devices based on DFA and TFA are comparable to the device based on NPB at the same driving voltage. Moreover, the device based on TFA achieved a maximum luminance of 89475 cd/m^2 at 11 V.

From Fig. 6a), it can be seen that, the maximum current efficiency of devices based on DFA, TFA and NPB were 31.26 cd/A, 41,68 cd/A and 29.92 cd/A, respectively, and the corresponding maximum power efficiency were 22.76 lm/W, 32.04 lm/W and 29.64 lm/W. Fig. 6c) implied that the maximum external quantum efficiencies were 8.86%, 12.04% and 8.70% for DFA, TFA and NPB based devices, respectively. Fig. 6a–c indicated that the efficiencies roll-off phenomena of devices based on DFA and TFA are somewhat alleviated comparing with NPB, which could be ascribed to the better hole-transport characteristics of these two compounds and more balanced charge combination properties of the DFA and TFA

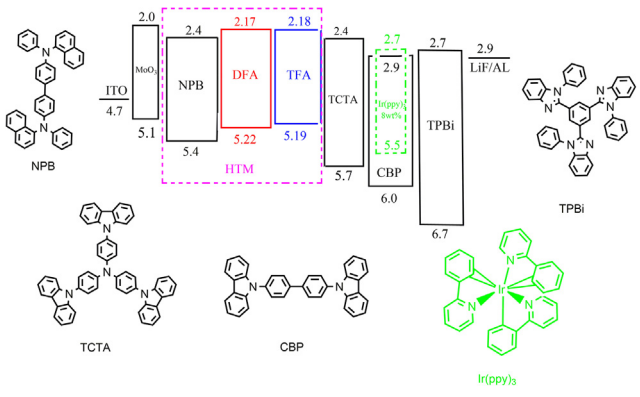

Fig. 4. The energy level diagram of the materials in devices.

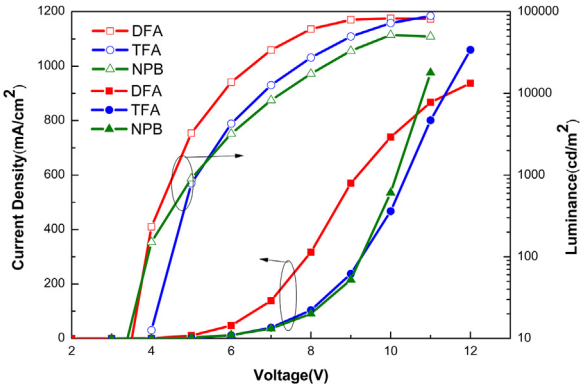

Fig. 5. Current density-voltage-luminance (I-V-L) curves of devices based on DFA, TFA and NPB.

Table 2
EL performance of devices based on **NPB**, **DFA** and **TFA**.

Compounds	V_{on}(V)[a]	L_{max}[cd/m^2][b]	η_c(cd/A)[c]	η_p(lm/W)[c]	η_{ext}(%)[c]	CIE$_{(x,y)}$[d]
NPB	2.9	51890	29.92	29.64	8.70	(0.44,0.28)
DFA	3.1	82530	31.26	22.76	8.86	(0.31,0.62)
TFA	3.6	89475	41.68	32.04	12.04	(0.31,0.61)

[a] Turn-on voltage to give a luminance of 1 cd/m^2.
[b] L_{max}: maximum luminance.
[c] Maximum values. η_c: current efficiency. η_p: power efficiency. η_{ext}: external quantum efficiency.
[d] Measured form the EL spectra at 10 V by inverting chromaticity coordinates on the CIE 1931 diagram.

based devices. Besides, the TFA-based device displays higher efficiencies than the DFA-based device as a result of stronger electron donating properties of triphenylamine moiety.

Fig. 7 showed the EL spectra of DFA and TFA based devices at 10 V. Emission at 516 nm and 512 nm respectively for DFA and TFA based devices can be seen clearly, which correspond to the CIE coordinates of (0.31, 0.62) and (0.31,0.61), respectively.

Hence, as revealed in Fig. 6 and Table 2, the devices based on DFA and TFA exhibited better performance than NPB, which could be attributed to the higher HOMO energy levels and excellent thermal stability of DFA and TFA.

3. Conclusion

To conclude, two novel hole transport materials based on naphtho[2,1-*b*]benzofuran were synthesized and well characterized. The good thermal stabilities and suitable HOMO energy levels of these two compounds allow them to be promising hole transport materials. In the test of the EL performance, DFA- and TFA-based devices showed better performance than NPB-based device. Especially, the TFA-based device exhibited the best performance with the current efficiency, power efficiency and external quantum efficiency of 41.68 cd/A, 32.04 lm/W and 12.04%, respectively, which proved that the introduction of naphtho[2,1-*b*]benzofuran can enhance the thermal stability and hole transport ability of triarylamine-based compounds. Thus, TFA will be a potential hole transport material for commercial application in OLEDs.

4. Experimental section

4.1. General information

All chemicals and solvents of the route were purchased from Shanghai Taoe chemical technology Co., Ltd and used as received without further purification. The ^{1}H and ^{13}C NMR spectra were recorded on a Bruker AM 400 spectrometer at room temperature. High resolution mass spectra were obtained by a Waters LCT premier XE spectrometer. The UV–vis absorption spectra and Photoluminescence (PL) spectra were recorded on a Varian Cary 500 spectrophotometer and a Varian-Cary fluorescence spectrophotometer, respectively. The cyclic voltammograms of the compounds were performed by a Versastat II electrochemical workstation using a conventional three electrode configuration with a glassy carbon

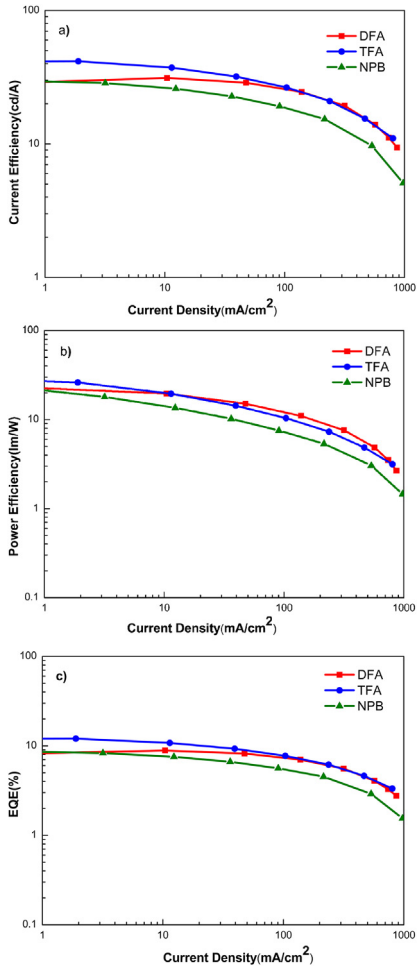

Fig. 6. a) current efficiency-current density curves; b) power efficiency-current density curves; c) external quantum efficiency-current density of devices based on DFA, TFA and NPB.

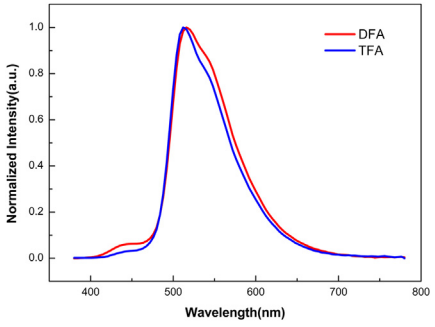

Fig. 7. EL spectra at 10 V of DFA- and TFA-based devices.

working electrode, a Pt wire counter electrode, and a regular calomel reference electrode in saturated KCl solution, 0.1M Bu_4NPF_6 in dichloromethane solution as a supporting electrolyte. Thermogravimetric analysis (TGA) were performed under a nitrogen atmosphere on a NETZSCH STA 409 PC/PG instrument and a TGA instrument. The differential scanning calorimetry (DSC) analysis were measured on a DSC Q2000 instrument under a nitrogen atmosphere.

4.2. Synthesis

4.2.1. Synthesis of N-([1,1'-biphenyl]-4-yl)-N-(4-bromophenyl)-9,9-dimethyl-9H-fluoren-2-amine (1)

A mixture of N-([1,1'-biphenyl]-4-yl)-9,9-dimethyl-9H-fluoren-2-mine (1.00 g, 2.77 mmol), 1-bromo-4-iodobenzene (1.00 g, 3,53 mmol), potassium hydroxide (0.30 g, 5.38 mmol), coprous iodide (5.70 mg, 0.03 mmol) and 1,10-Phenanthroline monohydrate (5.40 mg, 0.03 mmol) in ortho-xylene (30 mL) was stirred at 150 °C for 8 h under nitrogen atmosphere. After cooling to room temperature, the solution was evaporated in vacuum. The cold water was added to the mixture and finally extracted with DCM. The combined organic phase was collected, filtered and dried over $MgSO_4$. The crude product was purified by SiO_2 column chromatography using petroleum ether/dichloromethane (4:1, v/v) afforded **1** (1.31 g, 91.8%). ^{1}H NMR (400 MHz, $CDCl_3$) δ 7.58 (d, J = 7.5 Hz, 1H), 7.52 (t, J = 7.5 Hz, 3H), 7.43 (d, J = 8.7 Hz, 2H), 7.35 (dd, J = 15.4, 7.4 Hz, 3H), 7.29 (d, J = 8.9 Hz, 2H), 7.23 (m, 3H), 7.14 (d, J = 2.0 Hz, 1H), 7.10 (d, J = 8.6 Hz, 2H), 6.98 (m, 3H), 1.36 (s, 6H).

4.2.2. Synthesis of 7-bromo-N-(9,9-dimethyl-9H-fluoren-2-yl)-9,9-dimethyl-N-phenyl-9H-fluoren-2-amine (2)

A mixture of 9,9-dimethyl-N-phenyl-9H-fluoren-2-amine (2.00 g, 7.02 mmol), 2,7-dibromo-9,9-dimethyl-9H-fluorene (2.95 g, 8.43 mmol), potassium tert-butylate (1.56 g, 13.92 mmol), palladium acetate (40.41 mg, 0.18 mmol) and 2-dicyclohexylphosphino-2′,4′,6'-triisopropylbipheny (0.16 g, 0.36 mmol) was dissolved in 1,3,5-trimethylbenzene (30 mL) and heated at 170 °C for 7 h under nitrogen. After cooling to room temperature, the solution was evaporated in vacuum. The cold water was added to the mixture and finally extracted with DCM. The combined organic phase was collected, filtered and dried over $MgSO_4$. The crude product was purified by SiO_2 column chromatography using petroleum ether/dichloromethane (10:1, v/v) afforded **2** (1.82 g, 46.8%).^{1}H NMR (400 MHz, DMSO-d_6) δ 7.77–7.73 (m, 3H), 7.69 (d, J = 8.1 Hz, 1H), 7.53–7.49 (m, 2H), 7.38–7.22 (m, 7H), 7.14–7.08 (m, 3H), 6.99–6.95 (m, 2H), 1.36 (s, 12H).

4.2.3. Synthesis of naphtho[2,1-b]benzofuran-6-ylboronic acid (3)

A mixture of N,N,N′,N′-Tetramethylethylenediamine (4.68 g, 40.34 mmol) and dried tetrahydrofuran (100 mL) were added into a three-necked flask under a nitrogen atmosphere and stirring for 15 min under −78 °C, then 2.5M n-butyllithium (16.15 mL, 40.37 mmol) were added to the mixture by a disposable syringe and continue to stirring for 30 min. Subsequently, naphtho[2,1-*b*] benzofuran (8.00 g, 36.70 mmol) dissolved in tetrahydrofunan (50 mL) were added dropwise to the reaction stirring for 2 h. Finally, Boric Acid Triisopropyl Ester (18.74 mL, 80.73 mmol) were added to the mixture and continue to reacting for 2 h and resulting mixture was reacted overnight at room temperature. After cooling to ambient temperature, the mixture was extracted with water and dichloromethane, the organic layer was evaporated in vacuum affording white solid 5 (9.2 g, 95.7%).^{1}H NMR (400 MHz, $CDCl_3$) δ 8.62 (d, J = 8.3 Hz, 1H), 8.50 (s, 1H), 8.42 (m, J = 9.0 Hz, 1H), 8.11 (d, J = 8.2 Hz, 1H), 7.76 (m, 2H), 7.55 (m, 3H), 5.68 (s, 2H).

4.2.4. Synthesis of N-([1,1'-biphenyl]-4-yl)-9,9-dimethyl-N-(4-(naphtho[2,1-b]benzofuran-6-yl)phenyl)-9H-fluoren-2-amine (DFA)

A mixture of compounds 3 (0.3 g, 1.14 mmol), 1 (0.5 g, 0.97 mmol) and 2M aq.K_2CO_3 (10 mL) was stirred for 30 min under nitrogen atmosphere. Tetrakis(triphenylphosphine)palladium (0.023 g, 0.02 mmol) was added to the mixture, and the resulting mixture was refluxed for 6 h under nitrogen atmosphere. After cooling to room temperature, poured into H_2O and then extracted with dichloromethane. The combined organic phase was collected, filtered and dried over $MgSO_4$. The crude product was purified by SiO_2 column chromatography using petroleum ether/dichloromethane (4:1, v/v) afforded DFA (0.43 g, 68.0%). ^{1}H NMR (400 MHz, $CDCl_3$) δ 8.66 (d, J = 8.6 Hz, 1H), 8.46 (d, J = 8.9 Hz, 1H), 8.06 (d, 2H), 7.96 (d, J = 8.6 Hz, 2H), 7.73 (dd, J = 8.6, 5.2 Hz, 2H), 7.70–7.61 (m, 4H), 7.57 (d, J = 8.6 Hz, 3H), 7.53–7.49 (t, 2H), 7.44 (dd, J = 14.9, 7.2 Hz, 3H), 7.35 (m, 8H), 7.21 (d, J = 8.2 Hz, 1H), 1.47 (s, 6H). ^{13}C NMR (101 MHz, $CDCl_3$) δ 154.75, 154.19, 152.57, 151.17, 146.67, 145.99, 145.76, 139.53, 137.85, 134.49, 133.74, 129.89, 129.07, 128.76, 128.16, 127.74, 127.19, 126.85, 125.97, 125.86, 125.81, 125.77, 125.65, 125.58, 125.31, 124.91, 123.94, 123.70, 123.39, 123.05, 122.45, 122.20, 121.47, 120.96, 119.75, 118.50, 118.29, 116.98, 111.04, 45.88, 26.08. HRMS (ESI, m/z): $[M+H]^+$ calculated for $C_{49}H_{36}NO$, 654.2797, found 654.2784.

4.2.5. Synthesis of N-(9,9-dimethyl-9H-fluoren-2-yl)-9,9-dimethyl-7-(naphtho[2,1-b]benzofuran-6-yl)-N-phenyl-9H-fluoren-2-amine (TFA)

TFA (0.45 g, 92.53%) was synthesized in a similar way of DFA with **2** instead of **1**. ^{1}H NMR (400 MHz, $CDCl_3$) δ 8.60 (d, J = 8.2 Hz, 1H), 8.39 (d, J = 9.0 Hz, 1H), 8.03 (d, J = 5.2 Hz, 2H), 7.92 (d, J = 6.4 Hz, 2H), 7.76 (d, J = 8.0 Hz, 1H), 7.65 (d, J = 16.7 Hz, 2H), 7.54 (m, 5H), 7.44 (d, J = 10.7 Hz, 2H), 7.32 (d, J = 7.4 Hz, 1H), 7.23 (m, 6H), 7.16 (s, 1H), 7.07–6.98 (m, 3H), 1.46 (s, 6H), 1.36 (s, 6H). ^{13}C NMR (101 MHz, $CDCl_3$) δ 154.78, 154.41, 153.99, 152.94, 152.47, 151.24, 138.06, 137.96, 133.36, 129.89, 128.21, 127.59, 127.31, 127.14, 126.36, 126.25, 125.95, 125.89, 125.41, 124.91, 123.99, 123.73, 123.35, 122.25, 122.20, 122.14, 121.79, 121.45, 120.98, 119.79, 119.57, 118.51, 118.36, 117.56, 117.15, 117.00, 111.08, 46.01, 45.79, 26.12, 26.02. HRMS (ESI, m/z): $[M+H]^+$ calculated for $C_{52}H_{40}NO$, 694.3110, found 694.3103.

Acknowledgements

Q. Dong acknowledges the financial support from the National Natural Science Foundation of China (Grant No.: 61307030, 21402110). This work was also supported by the Program for the Outstanding Innovative Teams of Higher Learning Institutions of Shanxi (OIT), the Youth “Sanjin” Scholar Program, the Key R&D Project of Shanxi Province (International cooperation program, No. 201603D421032), Fund Program for the Scientific Activities of Selected Returned Overseas Professionals in Shanxi Province the Outstanding Young Scholars Cultivating Program and Research Project Supported by Shanxi Scholarship Council of China (Grant No.: 2014-02).

Appendix A. Supplementary data

Supplementary data related to this article can be found at http://dx.doi.org/10.1016/j.tet.2017.06.031.

References

1. Tang CW, VanSlyke SA. *Appl Phys Lett*. 1987;51:913–915.
2. Huang JH, Su JH, Tian H. *J Mater Chem*. 2012;22:10977–10989.
3. Zheng ZW, Dong QC, Gou L, Su JH, Huang JH. *J Mater Chem*. 2014;2:9858–9862.
4. Xia CY, Wang XM, Lin J, Jiang WL, Ni L, Huang W. *Synth Met*. 2009;159:194–200.

5. Forrest SR. *Nature*. 2004;428:911–918.
6. Gao H, Song J, Zhang XW, Shang SB, Song ZQ. *Tetrahedron*. 2013;69:8405–8411.
7. Sheats JR. *Science*. 1997;277:191–192.
8. Hebner TR, Wu CC, Marcy D, Lu MH, Sturm JC. *Appl Phys Lett*. 1998;72:519–521.
9. Baldo MA, Lamansky S, Burrows PE, Thompson ME, Forrest SR. *Appl Phys Lett*. 1999;75:4–6.
10. Chen HW, Liang WQ, Chen Y, et al. *Rsc Adv*. 2015;5:70211–70219.
11. Wu CC, Chen CW, Lin CL, Yang CJJ. *Disp Technol*. 2005;1:248–266.
12. Lee MT, Liao CH, Tsai CH, Chen CH. *Adv Mater*. 2005;17:2493–2497.
13. Thangthong A, Meunmart D, Prachumrak N, et al. *Chem Commun*. 2011;47:7122–7123.
14. Kelley TW, Baude PF, Gerlach C, et al. *Chem Mater*. 2004;16:4413–4416.
15. Kochapradist P, Prachumrak N, Tarsang R, et al. *Tetrahedron Lett*. 2013;54:3683–3687.
16. Tian GJ, Jiang YX, Wu P, et al. *New J Chem*. 2016;10:1039.
17. Hou XY, Li TC, Yin CR, Xu H, Lin J, Hua YR. *Synth Met*. 2009;159:1055–1057.
18. Lu J, Tao Y, D'iorio M, Li Y, Ding J, Day M. *Macromolecules*. 2004;37:2442–2448.
19. Balaji G, Parameswaran M, Jin TM, Vijila C, Furong Z, Valiyaveettil S. *J Phys Chem C*. 2010;114:4628–4630.
20. Promarak V, Ichikawa M, Meunmart D, Sudyoadsuk T, Saengsuwan S, Keawin T. *Tetrahedron Lett*. 2006;47:8949–8952.
21. Xiang N, Gao ZX, Tian GJ, et al. *Dyes Pigments*. 2017;137:36–42.
22. Yoo SJ, Jeon CW, Ha JJ, et al. *Macromol Res*. 2013;21:463–465.
23. Hreha RD, Haldi A, Domercq B, Barlow S, Kippelen B, Marder SR. *Tetrahedron*. 2004;60:7169–7176.
24. Omer KM, Ku SY, Wong KT, Bard AJ. *Angew Chem*. 2009;121:9464–9467.
25. Geng Y, Katsis D, Culligan SW, Ou JJ, Chen SH, Rothberg L. *J Chem Mater*. 2002;14:463–470.
26. VanSlyke SA, Chen CH, Tang CW. *Appl Phys Lett*. 1996;69:2160–2162.
27. Adachi C, Nagai K, Tamoto N. *Appl Phys Lett*. 1995;66:2679–2681.
28. Promarak V, Ichikawa M, Sudyoadsuk T, Saengsuwan S, Jungsuttiwong S, Keawin T. *Thin Solid Films*. 2008;516:2881–2888.
29. Kang JS, Hong TR, Kim HJ, et al. *J Mater Chem C*. 2016;4:4512–4520.